A Model of Phase Stability, Microstructure and Properties During Leaching of Portland Cement Binders

Pan Feng[a,b], Changwen Miao[b,c], Jeffrey W. Bullard[*,a,1]

[a] *National Institute of Standards and Technology, Gaithersburg, MD 20899, United States*
[b] *Southeast University, Nanjing, Jiangsu 210096, China*
[c] *Jiangsu Research Institute of Building Science Co., Ltd, Nanjing, Jiangsu 210008, China*

Abstract

A new model of 3D cement paste microstructure development is described and used to simulate the influence of leaching on hydrated cement pastes. In contrast to recent leaching models that have used empirical rules for phase dissolution, this model uses continual thermodynamic speciation and phase stability calculations to guide the microstructural changes that happen throughout hydration and subsequent exposure to low-pH solutions. This novel aspect of the model enables it to predict not only the well-known phase instability of calcium hydroxide at the onset of leaching, but also the detailed compositional and volumetric changes of C–S–H gel and other calcium, aluminate, and sulfate phases. Besides tracking the compositional and microstructural changes, we use the evolving microstructure as input to calculate changes in the relative diffusivity and effective Young's modulus of the binder using established finite difference and finite element models. The results are broadly consistent with previous experimental and modeling investigations of leaching. In particular, the leaching process can be roughly divided into initial, intermediate, and final stages, each of which have distinct degradation characteristics and consequences for mechanical and transport properties. The thermodynamic basis of the model makes it readily extensible to simulate a wide range of cementitious materials and degradation phenomena, so we discuss its potential as a virtual microprobe for use with continuum-scale service life models of concrete elements.

[*] Corresponding author
[1] Phone (301) 975-5725, Fax (301) 990-6891, Email jeffrey.bullard@nist.gov

Key words: cement paste, microstructure, leaching, computer modeling, elastic modulus, diffusivity

1. Introduction

Replacement or rehabilitation of existing concrete structures costs about $18 billion to $21 billion each year in the U.S. alone [1**?**]. Chemical deterioration of the cementitious binder is a primary reason for these high costs and represents a major challenge to increased sustainability of the civil infrastructure. Among the various kinds of chemical deterioration, leaching is a progressive extraction of calcium from the cementitious binder caused by contact with moisture having pH significantly lower than that of the alkaline pore solution [2]. As calcium leaches from concrete, its reactions with air or dissolved sulfates can cause efflorescence (*i.e.*, the surface formation of calcium carbonate or calcium sulfate). More importantly, the loss of calcium from the system also leads to dissolution of calcium hydroxide and a corresponding increase in porosity and transport properties of surface concrete [3, 4], so it can lead to accelerated degradation by other forms of chemical attack as well.

Investigations of leaching mechanisms by laboratory experiments are usually difficult and time consuming [5, 6], so a considerable effort has been spent on modeling the process. Bentz [3] and Marchand [7] both modeled the influence of the dissolution of portlandite (*i.e.*, calcium hydroxide) on pore structure and transport properties. Aspects of these models were incorporated into computational studies of the mechanical and transport properties of leached cement paste and mortar [8, 9, 10, 11, 12]. Berner [13] was perhaps the first to suggest the importance of thermodynamic equilibrium between the pore solution and the solid phases in the cement paste for determining the chemical evolution of a leached binder, and this concept has since been used in several models to describe the mass balance of calcium in the liquid and solid phases [14, 15, 16, 17, 18, 19]. Those kinds of models have provided considerable insight into the nature of leaching, its influence on capillary pore volume, and the corresponding changes in transport properties. Even so, the size distribution and connectivity of the capillary porosity, not just total pore volume, are important in determining transport properties. Furthermore, a detailed knowledge of the assemblage of solid phases in the binder microstructure can enable accurate calculations of composite properties (*e.g.*, elastic moduli, relative diffusivity) using 3D microstructure-based

software tools such as the Virtual Cement and Concrete Testing Laboratory (VCCTL) [20, 21].

In this paper, we extend a thermodynamically guided microstructure model of cement hydration [22] to simulate leaching of well-hydrated cement. The approach differs from previous models in three ways. First, we use full geochemical thermodynamic equilibrium calculations to assess both the volume fractions and compositions of the various solid binder phases and the speciation of the pore solution. Second, we link these equilibrium calculations to a digital-image model of 3D microstructure to track changes in the binder microstructure as leaching proceeds. And finally, we use the evolving microstructure explicitly to calculate, using finite element and finite difference models, the changes in Young's modulus and the relative diffusivity of the binder, respectively. In the remainder of the paper, we describe the modeling approach and apply it to simulate leaching of a Type I portland cement. Model predictions of chemical evolution, capillary porosity, Young's modulus, and relative diffusivity are presented and compared to results of previous experimental or modeling investigations.

1.1. Prior Investigations of Leaching

At least 15 previous studies of leaching, both experimental and modeling, have been reported in the past 20 years, using either plain calcium silicate systems [13, 14, 17] or portland cement systems [3, 4, 6, 7, 8, 9, 12, 15, 16, 23, 24]. In general, these investigations have observed three main stages of leaching in well-hydrated systems [9, 13, 17]:

- An *initial* stage, in which dilution of calcium, alkali, and hydroxyl ions in the leachate causes dissolution of portlandite (CH). During this stage, excess solid CH buffers the solution with respect to calcium and hydroxyl ions, thereby minimizing the dissolution of any other solid phases;

- An *intermediate* stage, which commences as soon as all CH has dissolved and can no longer buffer the solution. At this point the solution pH decreases and initiates the progressive decalcification of C–S–H gel [9, 13, 16, 17];

- A *final* stage, in which most of the calcium content of C–S–H has been lost, leaving behind a high-silica amorphous phase [13]. In principal, other low-solubility calcium aluminate phases may become unstable

and dissolve in this stage, too. Much of the material's original mass has been leached away by this stage, making it weak and subject to disintegration.

The computational model used in this paper recovers these three stages. In that sense, the current model does not reveal significantly new phenomena or mechanisms of leaching. However, with the model we are now able to analyze the coupling of the chemical evolution and accompanying changes in microstructure and properties that leaching causes. Modeling of leached microstructures and properties has been reported in the past [3, 9, 8], but lacked a firm basis in chemical thermodynamics to guide the accompanying phase changes, especially with regard to the decalcification of C–S–H and loss of aluminate phases. Part of our purpose in this paper, therefore, is to compare the results of the current model to those earlier results and to establish better ties between the chemical driving forces for leaching and the ensuing microstructure and property development. Moreover, the model, once validated for leaching phenomena, can be readily extended to analyze other types of degradation such as sulfate attack and carbonation.

2. Model Description and Technique

2.1. Simulation of hydration

The model used here is based on the Thermodynamic Hydration and Microstructure Evolution (THAMES) model recently developed at the National Institute of Standards and Technology (NIST) [22]. THAMES has three main components: (1) a kinetic model of cement clinker phase dissolution, which determines the time dependence of elemental concentrations in the pore solution; (2) thermodynamic equilibrium calculations to determine the composition and abundance of phases other than clinker minerals, including pore solution composition and speciation, corresponding to a minimum in Gibbs free energy; and (3) a digital image model for spatially distributing these various phases to represent the 3D microstructure of the binder. The dissolution rate of each of the four major clinker phases in portland cement (*i.e.*, C_3S, C_2S, C_3A, and C_4AF)[2] is calculated at each time interval using an empirical model proposed by Parrot and Killoh (PK) [25]. The PK

[2]Cement chemistry notation is used throughout, according to which C = CaO, S = SiO_2, A = Al_2O_3, and F = Fe_2O_3.

model uses equations to describe alternate mechanisms which could control the rate of hydration at any moment, including nucleation, growth of hydration phases, and diffusion of solute species. These rate equations depend on the instantaneous degree of hydration, the powder's specific surface area as measured by the Blaine fineness, the water-to-cement mass ratio (w/c), temperature, and six empirical parameters that are fit from observations on a wide range of portland cement pastes. The rate is calculated by evaluating the rate equation for each available mechanism and selecting the one that yields the minimum rate.

The thermodynamic component of THAMES is based on the GEMIPM2K thermodynamic model [26], supplemented with a thermodynamic database for the major minerals and hydration products found in cementitious materials [27]. This component is identical to that described elsewhere by Lothenbach [27, 28]. Briefly, everything except the clinker minerals is treated as a closed thermodynamic system; the clinker minerals are taken to be outside the thermodynamic system, and their extent of dissolution at any time sets the chemical composition of the thermodynamic system itself. Within the thermodynamic system, three types of matter are defined: (1) independent components (IC), which are chemical elements and electrical charge; (2) dependent components (DC), which are compounds or moieties composed of one or more ICs (*e.g.*, $Ca(OH)_2$, $SO^{2-}_{4(aq)}$); and (3) phases, which are composed of one or more DCs (*e.g.*, gypsum, aqueous solution). The model constrains the moles of each IC to be fixed at any time step, and the equilibrium distribution of the ICs among the possible DCs and phases, including solution speciation and partitioning of end members in solid solutions, is calculated by "dual-thermodynamic" calculations that minimize the Gibbs free energy [29]. At each time step, the instantaneous elemental composition of the pore solution, based on the amount of dissolution calculated in that time step by the PK model, defines the moles of each IC. Again, we repeat for clarity that the undissolved portions of the clinker phases are not part of the thermodynamic system.

An important point for this study is that the calcium silicate hydrate (C–S–H) gel is modeled as a nonstoichiometric phase with Ca/Si molar ratio varying continuously between 0 and 1.67, and its actual composition at equilibrium is determined by minimizing the Gibbs free energy according to the dual-thermodynamic methods used by the GEMIPM2K model. The solid solution model for C–S–H is similar to that proposed by Kulik and

Kersten [30]. Their original solid solution model was composed of two subsystems, a silica-rich subsystem with end members that are analogous to amorphous silica (Ca/Si = 0) and to a tobermorite-like form (Ca/Si = 0.83), and a calcium-rich subsystem with end members that are tobermorite-like (Ca/Si = 0.83) and jennite-like (Ca/Si = 1.67). However, recent NMR data indicate that C–S–H composition is captured more accurately by using only the calcium-rich solid solution subsystem for Ca/Si $\geq$ 0.8, which exists in equilibrium with amorphous silica for Ca/Si $<$ 0.8 [31]. The composition, molar masses, and molar volumes of these three components are shown in Table 1.

The 3D microstructure is modeled using a regular cubic lattice and assigning a single phase to each lattice site (or voxel) using a unique integer identifier for each phase. The initial microstructure of unhydrated cement paste was created using VCCTL software [20, 21], which uses generalized versions of NIST's CEMHYD3D models [32]. Complete details of how the virtual microstructure is generated, including particle size and shape distribution and statistical distribution of phases within multiphase particles, are provided elsewhere [32, 20]. The microstructure is modeled using 100 voxels in each dimension (*i.e.*, 10^6 total voxels), with each voxel having a volume of 1 μm^3. Voxels at interfaces between different phases are identified and stored in two different lists for each solid phase m. The dissolution list, $\{D\}_m$, is the set of voxels of solid phase m that are eligible to dissolve because they share at least one face or edge with a water voxel. Likewise, the growth list for solid phase m, $\{G\}_m$, is the set of water voxels that have at least one neighbor of solid phase m, and therefore are eligible to convert to solid phase m by accretion. Once the lists $\{D\}_m$ and $\{G\}_m$ are established, each member of each list is assigned an "affinity" for dissolution or growth, respectively, based on the phases defining the interface, the interface's local mean curvature [33], and a predefined tendency for a phase to adopt particular morphologies during hydration. For example, equiaxed growth morphologies can be produced by favoring the growth of solid voxels at interface regions of low mean curvature, while needle-like growth morphologies can be encouraged by favoring the growth of solid voxels at positions of high mean curvature.

At each time step, the thermodynamic calculation determines the predicted volume change of each solid phase in the microstructure, which is converted to a net change in the number of voxels of that phase. The microstructure is updated phase by phase by querying $\{D\}_m$ or $\{G\}_m$, to find the sites with greatest affinity for dissolution or growth, respectively. After

the dissolution and growth sites have been selected for a given time step, the affected voxels are changed to their new phases and the interface lists are updated accordingly. For example, dissolving voxels chosen from $\{D\}_m$ are switched from solid phase m to water. Likewise, growing voxels of phase m selected from the list $\{G\}_m$ are switched from water to solid phase m. If solid phase m is predicted to grow during a time step but $\{G\}_m$ is empty, then nucleation of that phase occurs. For phases like portlandite (CH) and ettringite, nucleation is assumed to occur randomly throughout the pore solution; for C–S–H, ample experimental evidence indicates that nucleation happens on the surface of clinker grains [34, 35], so the current model biases the nucleation probability to prefer clinker surfaces, as described fully in Ref. [22]. These procedures for dissolution, growth, and nucleation keep the volume fraction of each phase to within ±0.1 % of its equilibrium value.

2.2. Simulation of leaching

Fig.1 shows the general algorithm for the leaching model we use. The cementitious system is hydrated, using exactly the procedures already described in [22] to produce a mature simulated paste microstructure. At a predefined time—100 d of hydration in this paper— hydration is stopped and the simulation of leaching is started. The entire capillary pore space of the microstructure, including saturated and empty porosity, is filled at once with a dilute aqueous solution by extracting the calcium and alkali species. Ideally, one would like to accomplish this by simply modifying the molar concentrations of these species in the aqueous solution, but our thermodynamic model specifies input chemical composition solely in terms of the total moles of each IC for the whole system. The solution speciation is strictly an output of the equilibrium calculation, so it cannot be modified directly as input to the thermodynamic model. Therefore, we adopt a somewhat roundabout procedure for flushing the pore solution. First, the total mass of water in the aqueous solution phase is retrieved from the current equilibrium state, as are molal concentrations of Ca^{2+}, Na^{+}, and K^{+}. From these data, we calculate the number of moles of Na^{+}, K^{+}, and SO_4^{2-} that must be removed from the solution to reduce their molal concentrations each to 0.5 mmol/(kg water)or less, a value chosen to avoid numerical instabilities in the thermodynamic calculations while still enabling significant dilution of the solution. Next, we determine the number of moles of Ca^{2+} that must be removed from the solution to set its molar concentration to a prescribed value between 0.5 mmol/(kg water) and 20 mmol/(kg water). Finally, we

calculate the number of moles of OH^- that must be removed at the same time to maintain charge balance. From this information, we set the number of moles of the elements Ca, Na, K, O, and H corresponding to this dilution, re-calculate the equilibrium state, and update the microstructure accordingly. Note that in this dilution process, we ignore the presence of ion complexes such as $CaOH^+$, $CaSO_4^0$, and $NaOH^0$, which are typically present in significantly lower concentrations than the lone ions. The net elemental concentrations of calcium and alkali species will therefore be slightly greater than what we are approximating by this procedure, but this will have little impact on the driving force for leaching.

Equilibration of the diluted pore solution with the solids increases the concentration of calcium and alkali in solution as the solids partially dissolve, so the model repeats the process of flushing, re-equilibration, and microstructure updates until the equilibrium solution composition does not change appreciably with further cycles. The inevitable loss of solid volume due to leaching in any one of these cycles is replaced with an equal volume of water by adding the appropriate moles of H and O before the next cycle. The actual time associated with each of these leaching cycles would be determined by (1) the time required to exchange the pore solution with fresh solution, and (2) the time required for the fresh solution to reach equilibrium with the remaining solids. Either of these processes could, in principle, control the time scale of a given leaching cycle. In typical leaching experiments, dilution of the pore solution is accomplished by immersing the cement in a water bath of fixed composition, so solute diffusion from the interior capillary pore space probably controls the rate of leaching everywhere except very near the exterior surface, where the rate is likely controlled by mineral dissolution. The present simulations do not attempt to capture these kinetic complexities. Instead, we intend only to shed light on the overall course of degradation of the microstructure without reference to a particular time scale.

3. Results and Discussion

3.1. Cement paste composition and microstructure development

A Type I ordinary cement (proficiency sample cement 168 from the Cement and Concrete Reference Laboratory), was selected for these simulations. The cement has a fineness of 408 $m^2/kg \pm 10$ m^2/kg as measured by ASTM C 204 [36], with a median particle size of 13.7 μm as measured by

laser scattering from a dilute powder suspension in isopropanol. The mineralogical composition of the cement is shown in Table 1, and is based on average mass fractions obtained using X-ray powder diffraction with Rietveld refinement [22].

Virtual pastes based on this cement powder, with w/c of 0.40, 0.45, or 0.50 were constructed using VCCTL software. Sealed hydration of each paste for 100 d at a fixed temperature of 25 °C was simulated using the methods described in the previous section. The hydrated microstructures were then subjected to the iterative leaching algorithm. The microstructure, solid phase composition, and solution composition were tracked continuously during the simulation.

Fig. 2 shows the course of 3D microstructure development during hydration and leaching of a simulated paste with w/c = 0.45. The image (b) in this figure corresponds to the end of the 100 d hydration period. Fig. 3 shows the evolution of the capillary porosity and solid phases during the hydration period for the paste with w/c = 0.45, and Table 2 lists the predicted volume fractions, on a total volume basis, of the porosity, clinker phases, and hydration products at the end of 100 d for all three pastes. Experimental measurements of the phase assemblage at this late age are not available for direct comparison, but experimental measurements at times up to 7 d have been made on this cement using XRD with Rietveld refinement and are consistent with the hydration kinetics predicted by this model, as described fully in a previous paper that focused on modeling the hydration of this cement [22].

The capillary porosity in all three pastes decreases rapidly during the first five days because of the nucleation and growth of solid hydration products in the solution and on the cement particles. After this initial period, the porosity decreases at a much slower rate, reflecting the lower rates of hydration at later ages. Continual decreases in hydration rates are caused in these simulations by the assumption of the PK kinetic model that formation and thickening of hydration product layers around the remaining clinker grains increasingly resists diffusive mass transport between the dissolving grains and the pore solution.

The primary objective of this paper is to examine the simulation of leaching in mature pastes, so we do not elaborate further on the as-hydrated microstructures or their properties. Complete details of simulated and measured hydrated microstructures and properties of this cement are available elsewhere [22].

Fig. 2 (c) and (d) show the microstructure of the hydrated paste with w/c = 0.45 at different stages of leaching, in which one may readily observe the disappearance of CH and increase in porosity. To analyze the composition more quantitatively, we begin by plotting the combined Ca/Si molar ratio of the solid phases as a function of calcium concentration in the leaching solution. The same kind of plot has been used in previous leaching studies [13, 17, 24], so Fig. 4 compares the results of our simulations both with experimental data collected on leaching from multiple studies in Ref. [14] and with an empirical model, shown as a dashed curve from Ref. [13].[3] The chemical equilibria between the solution and solids were found in our simulations to be effectively independent of w/c ratio over the range studied, as one would expect. Therefore, all our simulation results fall onto the single solid curve shown in Fig. 4. The plot confirms that the current leaching simulation results are within the range of the experimental data at every calcium concentration, although more toward higher Ca/Si values than the majority of the measurements. However, it is important to note that the experimental data in the plot were obtained on calcium silicate hydrates composed of C–S–H gel and, at higher calcium concentrations, portlandite (CH). The current simulations were made on portland cement pastes, so our calculations of the solid phase Ca/Si ratio include not only C–S–H and CH but also small amounts of other calcium-bearing phases with no silicate component such as ettringite, monosulfate, and hydrotalcite. As such, one would expect the current simulations to yield slightly larger Ca/Si values than measurements obtained on pure calcium silicate systems.

One can discern three major stages of leaching in the shape of the curve shown in Fig. 4, as described in the Introduction. At the highest calcium concentrations in solution, about 18 mmol/(kg water) to 20 mmol/(kg water), leaching begins by progressive dissolution of solid CH. In Fig. 4 this is indicated by a decrease in Ca/Si ratio in the solids at constant calcium concentration. After all the CH dissolves, it can no longer buffer the calcium and hydroxyl ions in solution. Thereafter, a gradual decrease in Ca/Si ratio of the solids is observed with decreasing calcium concentration in solution. We call this behavior intermediate-stage leaching, and it is due primarily to

[3]The experimental data and the empirical model in the plot express solution concentration in units of mmol/(L solution) instead of mmol/(kg water). At the dilute concentrations of the leaching solutions, there is a negligible difference between these two sets of units.

decalcification of C–S–H gel. Fig. 5 shows that the volume fraction of C–S–H decreases steadily during this stage, while every other solid hydration product retains a nearly constant volume fraction. If C–S–H was dissolving at constant composition, the combined Ca/Si ratio of solids would be increasing because it is the only silicate-bearing phase in the system. Therefore, the C–S–H itself must be undergoing decalcification so that its Ca/Si ratio of remaining C–S–H decreases throughout the intermediate stage. When much of the calcium has been leached from C–S–H, at a solution concentration of about 2 mmol/(kg water), there is another steep change in solid Ca/Si ratio. We call this final-stage leaching, and it is observed only at very low calcium concentrations and low pH. As shown in Fig. 5, the remainder of the C–S–H dissolves. In addition, the remaining low-solubility calcium phases, ettringite and hydrotalcite, also become unstable and dissolve.

The solid curve in Fig. 4 shows only the final equilibrium Ca/Si values after repeated flushing with the leaching solution until the calcium concentration in solution does not change. However, we can also obtain a picture of how leaching progresses as it approaches equilibrium with a low-calcium leaching solution. Figures 6 and 7 plot the hydrated phase volume fractions and the solution concentrations, respectively, as a function of the number of leaching cycles (*i.e.*, solution flushes) as the hydrated system is repeatedly flushed with a 0.5 mmol/(kg water) calcium solution. For approximately the first 2200 leaching cycles, portlandite steadily dissolves while the volume of every other phase remains constant. Afterward, the intermediate stage is characterized by a reduction of the calcium-rich end member with Ca/Si = 1.67 together with a partial replacement of its volume by the tobermorite-like end member with Ca/Si = 0.83. This behavior continues until approximately 4300 leaching cycles (provisional calcium concentration of 2 mmol/(kg water)), at which point the calcium-rich end member has dissolved completely and a smaller volume of the tobermorite-like end member has taken its place. Immediately afterward, as the provisional equilibrium calcium concentration decreases from 2 mmol/(kg water), the tobermorite-like end member itself becomes thermodynamically unstable and begins to dissolve, being partially replaced in this stage by amorphous silica. The conversion to amorphous silica is complete by approximately cycle 4800.

We emphasize that the C–S–H solid solution model is not intended to convey actual structural information about the material. Instead, the solid solution model is a thermodynamically consistent way to model the composition of C–S–H and its dependence on the chemical potential of calcium and

silicates in solution. It has been demonstrated to accurately reproduce such compositional dependences [30, 31]. More recent efforts have been directed at improving the correspondence of the solid solution model to the structure of C–S–H [37]. However, for our purposes in simulating the chemical degradation by leaching, such correspondence with molecular structure is not included.

3.2. Diffusivity and conductivity

A 3D finite difference model for solving Ohm's law on random composite media [38] was used to calculate the relative DC conductivity, σ_{r}, of the microstructure as leaching progresses. The relative conductivity is defined as

$$\sigma_{\mathrm{r}} \equiv \frac{\sigma}{\sigma_{\mathrm{o}}} \tag{1}$$

where σ is the DC conductivity of the paste and σ_{o} is the DC conductivity of the bulk pore solution at the same temperature. By its definition, σ_{r} is a dimensionless quantity that is a property of the microstructure. We also can define a similar dimensionless microstructure property, the relative diffusivity, D_{r}, of any solution component,

$$D_{\mathrm{r}} \equiv \frac{D}{D_{\mathrm{o}}} \tag{2}$$

where D is the diffusivity of some solution component in the paste and D_{o} is the diffusivity of that component in the bulk pore solution at the same temperature. Moreover, $D_{\mathrm{r}} \equiv \sigma_{\mathrm{r}}$ [39], and we state the results that follow in terms of D_{r}. In fact, for direct comparison with experimental measurements of calcium diffusivity in leached pastes by Mainguy [15], we approximate the effective diffusivity for calcium in the leaching solution by multiplying the calculated values of D_{r} by D_{o} for Ca^{2+} in water at infinite dilution at 25 °C, which is 7.92×10^{-10} m^2/s [40]. This is known to be a rough approximation because the effective diffusivity of ions in electrolytes varies considerably with composition and ionic strength.

In the current simulations, every phase in the microstructure was assumed to have a relative conductivity of zero except for saturated porosity ($D_{\mathrm{r}} = 1$ by definition) and C–S–H, which was assumed to have $D_{\mathrm{r}} = 0.0025$ based on prior modeling studies using digital image representations of cement paste microstructure [3, 41]. The changing structure and composition of C–S–H during leaching may likely influence its value of D_{r}, but we do not include

any such dependence for lack of experimental data on the magnitude of such changes.

Fig. 8 shows the calculated calcium diffusivity for the 0.40, 0.45, 0.50 w/c cement paste plotted against capillary porosity. The open diamonds are experimental data measured in Ref. [15], and the solid line shows the following empirical exponential relationship between the effective diffusivity and the capillary porosity, ϕ, proposed in that work:

$$D = e^{9.95\phi - 29.08} \tag{3}$$

The current leaching model agrees fairly well with the experimental measurements, within a factor of two at all points, although it appears to modestly overestimate the diffusivity at larger porosities. The model predictions appear to be consistent with the observations, considering the likely uncertainties in the reported experimental measurements and the fact that the cement paste modeled here differs from that used in the experimental work. In addition, our estimate of calcium ion diffusivity may be too high for leaching solutions with finite ionic strength [42], perhaps by as much as 15 %.

In the plot of diffusivity versus porosity in Fig. 8, the calculated values for all three w/c ratios fall very nearly on a single curve. The inset shows that this is not entirely accurate in the intermediate porosities of 0.2 to 0.4 (which is discussed below) but the overall behavior appears to be nearly independent of w/c. The curve shape in Fig. 8 reveals three distinct regions of behavior predicted by the model. First, at the lowest porosities (*i.e.*, initial stage of leaching), $\log(D)$ increases fairly linearly with porosity until reaching a porosity of about 0.20, above which the slope increases. Prior microstructure modeling studies using digitized images indicate a percolation threshold in capillary porosity at porosities in this same range [43, 44], and we expect that the sudden slope change in in Fig. 8 at 0.20 porosity is caused by this same phenomenon. To confirm this, we used a burning algorithm [45] to assess the connectivity of capillary porosity in the microstructures as a function of porosity both during hydration (decreasing porosity) and during leaching (increasing porosity). Fig. 9 shows the fraction of interconnected capillary porosity as a function of porosity for w/c = 0.50. The porosity clearly passes a percolation threshold at about 0.20. The influence on relative diffusivity is most noticeable for the paste with w/c = 0.4 because it is the only paste that began the leaching process with porosity significantly below 0.18. The pore percolation threshold is crossed during leaching due solely to the dissolution of CH, which leaves relatively large pores behind. Fig. 10 shows the

volume fraction of the major hydration products as a function of porosity as leaching progresses. It indicates that CH is not fully dissolved (for a w/c = 0.45) until the capillary porosity is about 0.28. Therefore, the pore percolation phenomenon is a feature of initial-stage leaching, and it has significant implications for the decreased resistance of the material to additional degradation; once the percolation threshold is crossed, further erosion of the solid products produce relatively greater changes in the diffusivity.

Bentz and Garboczi [3] reported a significant hysteresis in the percolation curves when modeling hydration and leaching with digitized microstructure models, and the effect became more pronounced with decreasing w/c ratio. In contrast, we observe little if any hysteresis in the curves at any of the three w/c ratios used in this study; the differences in Fig. 9 for w/c = 0.50 are typical and similar to those seen in Ref. [3] for w/c = 0.6. We are unaware of any experimental data to support or refute a significant hysteresis between hydration and leaching, and the differences in this regard between our model and that in Ref. [3] can likely be attributed to differences in the stochastic rules each model uses to distribute CH during hydration [3, 22]. However, although we observe minor hysteresis in the percolation of capillary porosity between hydration and leaching, there is a distinct difference between the calculated relative diffusivity of a hydrated microstructure and the leached microstructure at equal porosity, both below and above the pore percolation threshold during the initial stage of leaching. Fig. 11 indicates that, for all three w/c ratios studied, the leached microstructure exhibits greater relative diffusivity at any porosity than the hydrated microstructure at the same porosity. The effect is most pronounced at the lower w/c ratios and at lower porosities, as much as a factor of five for the w/c = 0.40 when the porosity is approximately 0.18. This behavior indicates that the pore network itself, even after crossing the percolation threshold, offers less resistance to diffusion at any leached porosity than in the hydrated microstructure at the same porosity. The minor hysteresis in percolation behavior is largely responsible for this, although we also expect that the pore size distribution of the interconnected porosity is weighted more toward larger pores during initial-stage leaching, when only large crystallites of CH are dissolving, than during hydration.

The second region of interest in Fig. 8 occurs in the porosity range of 0.2 to 0.4, during which an abrupt decrease in the slope of $\log(D)$ vs. porosity can be observed (see inset to Fig. 8). The porosity at which this change occurs increases with increasing w/c of the paste (*e.g.*, 0.22, 0.28, and 0.32

for w/c = 0.40, 0.45, and 0.50, respectively, indicated by the vertical dashed lines). We note that these are the porosities at which portlandite (CH) is completely consumed by leaching, as shown in Fig. 10 for the paste with w/c = 0.45. During hydration, CH forms in fairly large domains in the capillary porosity, so its ongoing dissolution during leaching opens up large pores that represent fast diffusion paths. When CH is fully consumed, further leaching of C–S–H happens rather uniformly throughout its finer morphology. The attending increases in porosity are in the form of finer and more tortuous pathways, so $\log(D)$ increases more gradually with leaching at these higher porosities. This change of slope therefore corresponds to the transition from initial-stage leaching (*i.e.*CH dissolution only) to intermediate-stage leaching (*i.e.*progressive decalcification of C–S–H).

The third region of behavior occurs for very high porosities (*i.e.*, intermediate-stage and final-stage leaching), at which the microstructure is progressively less able to resist diffusion and D converges to its value for the bulk solution. As noted earlier, these severely leached materials have very high porosities and can therefore be expected to be weak enough to easily disintegrate by mechanical abrasion. Therefore, it is unclear whether the final stage of leaching is ever reached in practice before failure of the material.

In comparing the calculated diffusivity values to earlier studies, we note that, in addition to the experimentally measured values from Ref. [15] shown in Fig. 8, a recent model of leaching [9] predicted values of D for a "well-hydrated" portland cement paste (w/c = 0.4), and for the same paste leached to the point of disappearance of CH, of 2.76×10^{-12} m^2/s and 8.66×10^{-11} m^2/s, respectively. These values both are comparable to the values calculated by this model for the paste with w/c = 0.40 (see Fig. 8). More detailed comparisons to that study [9] are not possible because that study did not report values of degree of hydration of the paste and because that study appears to have assumed a different ranking of phase instabilities after CH dissolution than the ranking calculated thermodynamically in the current study.

3.3. Young's modulus

A 3D finite element model tailored for computing linear elastic moduli of random composite media [38] was used to calculate the changes in Young's modulus, E, as a function of capillary porosity, during both hydration and subsequent leaching. As detailed in Ref. [38], the finite element model uses the full 3D microstructure as input, representing each voxel as a trilinear cubic mesh element. Each microstructure phase is assigned a value for its

Young's modulus and Poisson ratio; values of these properties for most cement phases have been generally accepted in the literature and are tabulated in Ref. [46]. In particular, the Young's modulus and Poisson's ratio for C–S–H are assumed to be 22.4 GPa and 0.25, respectively. These values may likely depend on C–S–H composition and structure [47, 48], both of which are changing significantly during leaching, but we lack reliable data for such an effect. Therefore, for simplicity we assume that the values of C–S–H moduli are fixed. Consequently, we expect that the model predictions of bulk Young's modulus may overestimate the actual value in the latter stages of leaching where severe calcium depletion is likely to compromise the mechanical integrity of the C–S–H gel.

Model calculations of E are summarized for all three w/c ratios in Fig. 12, where the open symbols are values calculated during hydration and the filled symbols connected by lines are values calculated during leaching. The figure indicates significant qualitative and quantitative differences in the dependence of E on porosity during hydration compared to leaching. Specifically, E increases approximately linearly as the porosity decreases during hydration, and the slope of the relation is about the same at each w/c ratio. At a given capillary porosity, the paste with lowest w/c has the greatest proportion of clinker minerals in the solid, which are stiffer than the hydration products, so the paste with lowest w/c has the greatest E at any porosity. This behavior is consistent with the results of an earlier modeling study of the influence of hydrated microstructure on linear elastic properties [46].

The dependence of E on porosity is significantly different during leaching. Fig. 12 indicates that the calculated moduli decrease more rapidly with increasing porosity during leaching than during hydration. Recall that, when leaching starts, the paste has been almost fully hydrated, so there is a negligible fraction of clinker phases in the microstructure. Therefore, the elastic stiffness of the paste is due primarily to C–S–H and CH. CH is the stiffer of these two phases, having a Young's modulus of 42.3 GPa [49, 50] compared to 22.4 GPa for C–S–H [46]. The loss of only CH in the early stage of leaching corresponds to a stronger dependence of E on porosity than is observed throughout hydration, when mostly C–S–H and some CH is precipitating in the pore space.

A second noticeable difference in the behavior of E during leaching is the abrupt decrease in slope at intermediate porosities in Fig. 12. Careful examination of the figure reveals that this change in slope occurs at a different porosity for each w/c ratio. In fact, the porosities at which the slope change

occurs (0.22, 0.28, and 0.32 for w/c = 0.40, 0.45, and 0.50, respectively) are the same as those observed for the relative diffusivity in Fig. 8. As described in the previous section, these are the porosities at which CH is completely leached from the microstructure, and continued leaching to higher porosities occurs by dissolution of C–S–H, which is more elastically compliant than CH. Therefore, replacement of C–S–H by porosity has less of an effect on the composite value of E than when CH is replaced by porosity in the early stage of leaching. Again, the details of the order in which phases are removed from the microstructure by leaching has a modest but noticeable influence on the evolution of transport and mechanical properties of the material.

This subsection and the previous one demonstrate how the evolving microstructure can be linked to the evolving mechanical and transport properties of the material, by direct input of the digital image microstructures in finite difference and finite element models that can compute the relative conductivity (or diffusivity) and linear elastic moduli, respectively. As expected qualitatively, the relative diffusivity increases and Young's modulus decrease with increasing extent of leaching, both trends being directly attributable to increases in capillary porosity. However, these properties have a distinctly different dependence on porosity during hydration, when the porosity is decreasing, than during leaching. These differences can be attributed to the physics of the two processes: hydration in its latter stages occurs by a gradual infilling of the smallest capillary pores by C–S–H, aluminosulphate phases, and portlandite, whereas the early stages of leaching are characterized by the formation of larger pores by the removal of large portlandite masses.

3.4. Leaching Kinetics

As a first step, this study has modeled leaching as a sequence of quasi-static steps from one equilibrium state to another by successive flushings of the pore solution with a dilute leaching solution. During each flushing step, the system was allowed to reach equilibrium before the next flushing step occurred, without regard to the length of time associated with that equilibration. However, in future studies it should be possible to model the kinetics of leaching more directly by accounting for the kinetics of dissolution of the solid phases. For example, early stage of leaching is characterized primarily by the dissolution of portlandite, so the time associated with each flushing cycle could be linked with the time required for dissolution of the amount of portlandite needed to achieve equilibrium with the pore solution.

The dissolution rate can be estimated by a classical first-order rate law,

$$\dot{N} = kS(1 - \frac{Q}{K}) \tag{4}$$

where $\dot{N}$ is the molar dissolution rate of portlandite, k is the dissolution rate constant (about 6.3 μmol/m^2/s for portlandite [51]), S the reactive surface area of portlandite, Q is the ion activity product $\{Ca^{2+}\}\{OH^-\}^2$, and K is the solubility product for the reaction $Ca(OH)_2 \longrightarrow Ca^{2+} + 2\,OH^-$, about 6.31×10^{-6}. The dissolution rate of portlandite could therefore be estimated by interrogating the microstructure to determine S. The value of Q is initially determined by the composition of the flushing solution at the beginning of each flushing cycle, but will gradually asymptote to K as equilibrium is approached. In like manner, the kinetics during the latter stages of leaching could be estimated by using estimates for the calcium leaching rate constant and solubility product of C–S–H.

3.5. Relation to Existing Leaching Models

Sophisticated computer models are available for predicting the performance and service life of concrete structural elements [52]. However, these kinds of models are macroscopic reaction-transport models that do not resolve the structure of the material either at the aggregate or cement paste scale. The connection of these models to material properties is therefore necessarily based on significant calibration to experimental data that establish, for example, the dependence of the transport properties on porosity. A modeling approach like that described here, which resolves structure-property relationships at the cement paste scale, offers an attractive supplement to macroscopic service life prediction models because it can calculate local microstructure, elastic properties, and transport properties at selected critical locations in the larger element. That is, the spatial distribution of important properties can be calculated and updated throughout the life of a concrete structure exposed to aggressive chemical environments. In this sense, the current modeling approach is not only a valuable tool for understanding microstructure-property relationships during chemical degradation, but also represents a "virtual microprobe" that can be used within the context of larger software packages for service life prediction, especially when the model has been enhanced to include portlandite dissolution kinetics as described earlier. In addition, the same ideas can be applied to simulate other degradation phenomena, such as sulfate attack, carbonation, and chloride binding

in portland cement binders. The microstructure model and the thermodynamic database already include the necessary information on phases such as Friedel's salt and brucite that characteristically form during these kinds of chemical attack. The growth forms and spatial distribution of these phases will need to be calibrated in the microstructure model based on comparison to experimental examination of microstructures with scanning electron microscopy or X-ray computed tomography, but the modeling approach itself should still be valid and could result in a generalized tool for simulating degradation in generalized service conditions.

4. Conclusion

We have demonstrated how a model which couples geochemical thermodynamic equilibrium calculations with a model of 3D cement paste microstructure can be applied to simulate both hydration and leaching of a Type I portland cement concrete binder. The simulations agree with prior studies that leaching of portland cement pastes occurs in three stages, beginning with the dissolution of portlandite, which can buffer the solution with respect to calcium at about 18 mmol/(kg water) until it is fully consumed (Stage 1). After the dissolution of portlandite, this buffering capability is lost and further leaching occurs by loss of C–S–H and a reduction in its Ca/Si molar ratio (Stage 2). Ultimately, when most of the calcium has been removed from C–S–H, at about 2 mmol/(kg water), the model indicates that the remaining low-solubility calcium-bearing phases such as ettringite and hydrotalcite become unstable and dissolve, leaving behind an amorphous silica remnant of the original C–S–H as the only solid phase (Stage 3). If exchange between the leaching solution and the interior is slow enough that the pore solution can reach provisional equilibrium with the solid phases, the dissolution of ettringite and the remaining calcium in C–S–H can promote a transient driving force for precipitation of gypsum, although one expects this phenomenon to be quite brief.

In addition to simulating microstructure changes due to leaching, we have also applied finite element and finite difference models directly to the microstructures to calculate the changes in the elastic moduli and relative diffusivity of the binder, respectively. The calculated values of these properties, and how they change with progressive leaching, generally agree with measurements reported in the literature. Therefore, the current model provides an explicit link between the chemical driving forces for microstructure changes

and the consequences for material performance. Furthermore, the same thermodynamic database and microstructure modeling algorithms can be applied to simulate other degradation phenomena such as sulfate attack and carbonation. Current research to link the microstructure evolution to a physical time scale, by modeling the dissolution kinetics of portlandite and the rate of solute transport out of the system, should make this modeling approach useful as a virtual microprobe for calculating time dependent changes in local properties of structural elements in the context of macroscopic models of service life prediction.

5. Acknowledgments

The China Scholarship Council (CSC) provided financial support for PF. The authors are grateful to Ed Garboczi, Dale Bentz, and Barbara Lothenbach for insightful comments during the preparation of the manuscript.

References

[1] Vision 2020: A Vision for the Concrete Repair, Protection and Strengthening Industry. Farmington Hills, MI: ACI Strategic Development Council; 2006.

[2] Roziere, E., Loukili, A., El-Hachem, R., Grondin, F.. Durability of concrete exposed to leaching and external sulphate attacks. Cem Concr Res 2009;39:1188–1198.

[3] Bentz, D.P., Garboczi, E.J.. Modelling the leaching of calcium hydroxide from cement paste: Effects on pore space percolation and diffusivity. Mater Struct 1992;25:523–533.

[4] Carde, C., Francois, R.. Modeling the loss of strength and porosity increase due to the leaching of cement pastes. Cem Concr Composites 1999;21:181–188.

[5] Adenot, F., Buil, M.. Modeling of the corrosion of the cement paste by deionized water. Cem Concr Res 1992;22:489–496.

[6] Delagrave, A., Gerard, G., Marchand, J.. Modeling the calcium leaching mechanisms in hydrated cement pastes. In: Mechanisms of Chemical Degradation of Cement-Based Materials. E & FN Spon; 1997, p. 38–49.

[7] Marchand, J., Bentz, D.P., Samson, E., Maltais, Y.. Influence of calcium hydroxide dissolution on the transport properties of hydrated cement systems. In: Skalny, J., Gebauer, J., Odler, I., editors. Materials Science of Concrete: Calcium Hydroxide in Concrete. Westerville, OH: American Ceramic Society; 2001, p. 113–129.

[8] Bernard, F., Kamali-Bernard, S., Prince, W.. 3d multi-scale modelling of mechanical behaviour of sound and leached mortar. Cem Concr Res 2008;38:449–158.

[9] Bernard, F., Kamali-Bernard, S.. Performance simulation and quantitative analysis of cement-based materials subjected to leaching. Computational Materials Science 2010;:in press.

[10] Guillon, E., Moranville, M., Kamali, S.. Characterization of the mechanical damage of a chemically degraded cement paste. Materials and Structures 2006;39:401–409.

[11] Kamali-Bernard, S., Bernard, F.. How to assess the long-term behaviour of a mortar submitted to leaching? European Journal of Environmental and Civil Engineering 2011;15:1031–1034.

[12] Kamali, S., Moranville, M., Leclercq, S.. Material and environmental parameter effects on the leaching of cement pastes: Experiments and modelling. Cem Concr Res 2008;38:575–585.

[13] Berner, U.R.. Modelling the incongruent dissolution of hydrated cement minerals. Radiochimica Acta 1988;44/45:387–393.

[14] Berner, U.R.. Evolution of pore water chemistry during degradation of cement in a radioactive waste repository environment. Waste Management 1992;12:201–219.

[15] Mainguy, M., Tognazzi, C., Torrenti, J.M., Adenot, F.. Modelling of leaching in pure cement paste and mortar. Cem Concr Res 2000;30:83–90.

[16] Nakarai, K., Ishida, T., Maekawa, K.. Modeling of calcium leaching from cement hydrates coupled with micro-pore formation. J Adv Concr Tech 2006;4(3):395–407.

[17] Gérard, B., Le Bellego, C., Bernard, O.. Simplified modelling of calcium leaching in concrete in various environments. Mater Struct 2002;35:632–640.

[18] Gawin, D., Pesavento, F., Schrefler, B.A.. Modeling of cementitous materials exposed to isothermal calcium leacing, considering process kinetics and advective water flow. Part I: Theoretical model. Intl J Solids and Structures 2008;45:6221–6240.

[19] Gawin, D., Pesavento, F., Schrefler, B.A.. Modeling deterioration of cementitious materials exposed to calcium leaching in non-isothermal conditions. Comput Methods Appl Mech Engrg 2009;198:3051–3083.

[20] Bullard, J.W., Stutzman, P.E.. Analysis of CCRL Portland cement proficiency samples number 151 and number 152 using the virtual cement and concrete reference laboratory. Cem Concr Res 2006;36:1548–1555.

[21] Sahachaiyunta, P., Ponpaisanseree, K., Bullard, J.W., Stutzman, P.E., Garboczi, E.J., Vichit-Vadakan, W.. Virtual testing in a cement plant. Concr Intl 2012;:33–39.

[22] Bullard, J.W., Lothenbach, B., Stutzman, P.E., Snyder, K.A.. Coupling thermodynamics and digital image models to simulate hydration and microstructure development of portland cement pastes. J Mater Res 2011;26(4):609–622.

[23] Gaitero, J.J., Campillo, I., Guerrereo, A.. Reduction of the calcium leaching rate of cement paste by addition of silica nanoparticles. Cem Concr Res 2008;38:112–118.

[24] Jain, J., Neithalath, N.. Analysis of calcium leaching behavior of plain and modified cement pastes in pure water. Cem Concr Composites 2009;31:176–185.

[25] Parrot, L.J., Killoh, D.C.. Prediction of cement hydration. Brit Ceram Proc 1984;35:41–53.

[26] Kulik, D.A.. GEMS-PSI 2.03, http://gems.web.psi.ch. 2009. URL: `http://gems.web.psi.ch`.

[27] Lothenbach, B., Winnefeld, F.. Thermodynamic modelling of the hydration of Portland cement. Cem Concr Res 2006;36:209–226.

[28] Lothenbach, B., Matschei, T., Möschner, G., Glasser, F.P.. Thermodynamic modelling of the effect of temperature on the hydration and porosity of Portland cement. Cem Concr Res 2008;38:1–18.

[29] Kulik, D.A.. Dual-thermodynamic estimation of stoichiometry and stability of solid solution end members in aqueous-solid solution systems. Chem Geology 2006;225(3–4):189–212.

[30] Kulik, D.A., Kersten, M.. Aqueous solubility diagrams for cementitious waste stabilization systems. II, end-member stoichiometries of ideal calcium silicate hydrate solid solutions. J Am Ceram Soc 2001;84(12):3017–3026.

[31] Lothenbach, B., Le Saout, G., Ben Haha, M., Figi, R., Wieland, E.. Hydration of a low-alkali CEM III/B-SiO_2 cement (LAC). Cem Concr Res 2012;42:410–423.

[32] Bentz, D.P.. Three-dimensional computer simulation of cement hydration and microstructure development. J Am Ceram Soc 1997;80(1):3–21.

[33] Bullard, J.W., Garboczi, E.J., Carter, W.C., Edwin R. Fuller, J.. Numerical methods for computing interfacial mean curvature. Comput Mater Sci 1995;4:103–116.

[34] Bullard, J.W., Jennings, H.M., Livingston, R.A., Nonat, A., Scherer, G.W., Schweitzer, J.S., et al. Mechanisms of cement hydration. Cem Concr Res 2011;41(12):1208–1223.

[35] Gartner, E.M., Young, J.F., Damidot, D.A., Jawed, I.. Hydration of Portland cement. In: Bensted, J., Barnes, P., editors. Structure and Performance of Cements; 2 ed. New York: Spon Press; 2002, p. 57–113.

[36] Annual Book of ASTM Standards; vol. 04.01. West Conshohocken, PA: ASTM International; 2000.

[37] Kulik, D.A.. Improving the structural consistency of C–S–H solid solution thermodynamic models. Cem Concr Res 2011;41:477–495.

[38] Garboczi, E.J.. Finite element and finite difference programs for computing the linear electric and elastic properties of digital images of random materials. NISTIR 6269; U.S. Department of Commerce; 1998.

[39] Snyder, K.A.. The relationship between the formation factor and the diffusion coefficient of porous materials saturated with concentrated electrolytes: Theoretical and experimental considerations. Concr Sci Eng 2001;3:216–224.

[40] Sugiyama, T., Ritthichauy, w., Tsuji, Y.. Simultaneous transport of chloride and calcium ions in hydrated cement systems. J Adv Concr Tech 2003;1:127–138.

[41] Garboczi, E.J., Bentz, D.. Computer simulation of the diffusivity of cement-based materials 1992;27:2083–2092.

[42] Snyder, K.A., Feng, X., Keen, B.D., Mason, T.O.. Estimating the electrical conductivity of cement paste pore solutions from OH^-, K^+, and Na^+ concentrations. Cem Concr Res 2003;33(6):793–798.

[43] Bentz, D.P., Garboczi, E.J.. Percolation of phases in a three-dimensional cement paste microstructural model. Cem Concr Res 1991;21(2):325–344.

[44] Garboczi, E.J., Bentz, D.P.. The effect of statistical fluctuation, finite size error, and digital resolution on the phase percolation and transport properties of the NIST cement hydration model. Cem Concr Res 2001;31:1501–1514.

[45] Stauffer, D., Aharony, A.. Introduction to Percolation Theory. 2 ed.; London: Taylor and Francis; 1994.

[46] Haecker, C.J., Garboczi, E.J., Bullard, J.W., Bohn, R.B., Sun, Z., Shah, S.P., et al. Modeling the linear elastic properties of Portland cement paste. Cem Concr Res 2005;35:1948–1960.

[47] Constantinides, G., Ulm, F.J.. The effect of two types of C–S–H on the elasticity of cement-based materials: Results from nanoindentation and micromechanical modeling. Cem Concr Res 2004;34(1):67–80.

[48] Shahsavari, R., Buehler, M.J., Pellenq, R.J.M., Ulm, F.J.. First-principles study of elastic constants and interlayer interactions of complex hydrated oxides: Case study of tobermorite and jennite. J Am Ceram Soc 2009;92(10):2323–2330.

[49] Holuj, F., Drozdowski, M., Czajkowski, M.. Brillouin spectrum of $Ca(OH)_2$. Solid State Commun 1985;56:1019–1021.

[50] Monteiro, P.J.M., Chang, C.T.. The elastic moduli of calcium hydroxide. Cem Concr Res 1995;25:1605–1609.

[51] Bullard, J.W., Flatt, R.J.. New insights into the effect of calcium hydroxide precipitation on the kinetics of tricalcium silicate hydration. J Am Ceram Soc 2010;93(7):1894–1903.

[52] Marchand, J., Samson, E., Maltais, Y.. Predicting the performance of concrete structures exposed to chemically agressive environment-field validation. Mater Struct 2002;35:623–631.

List of Figures

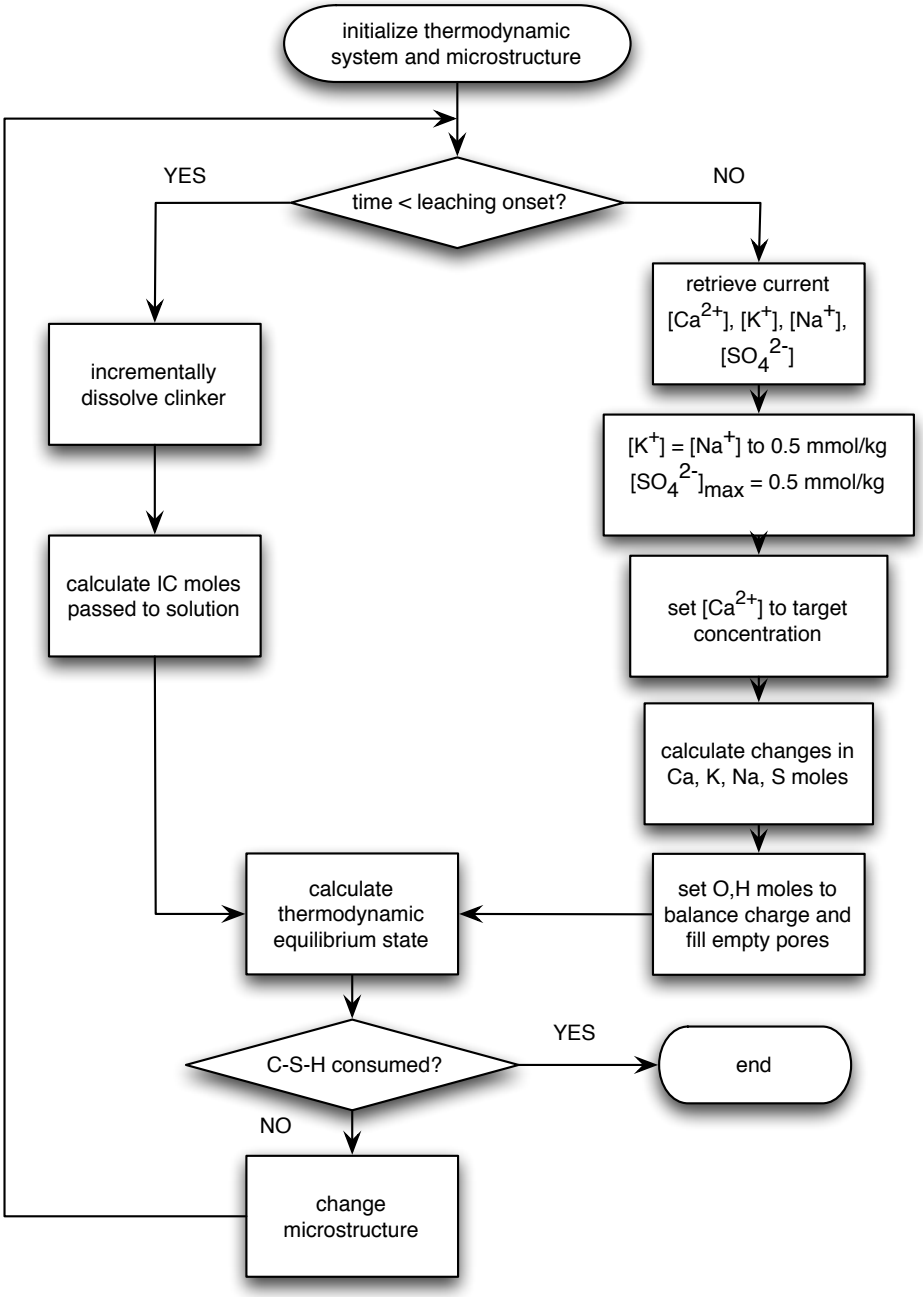

Figure 1: Flowchart of leaching model

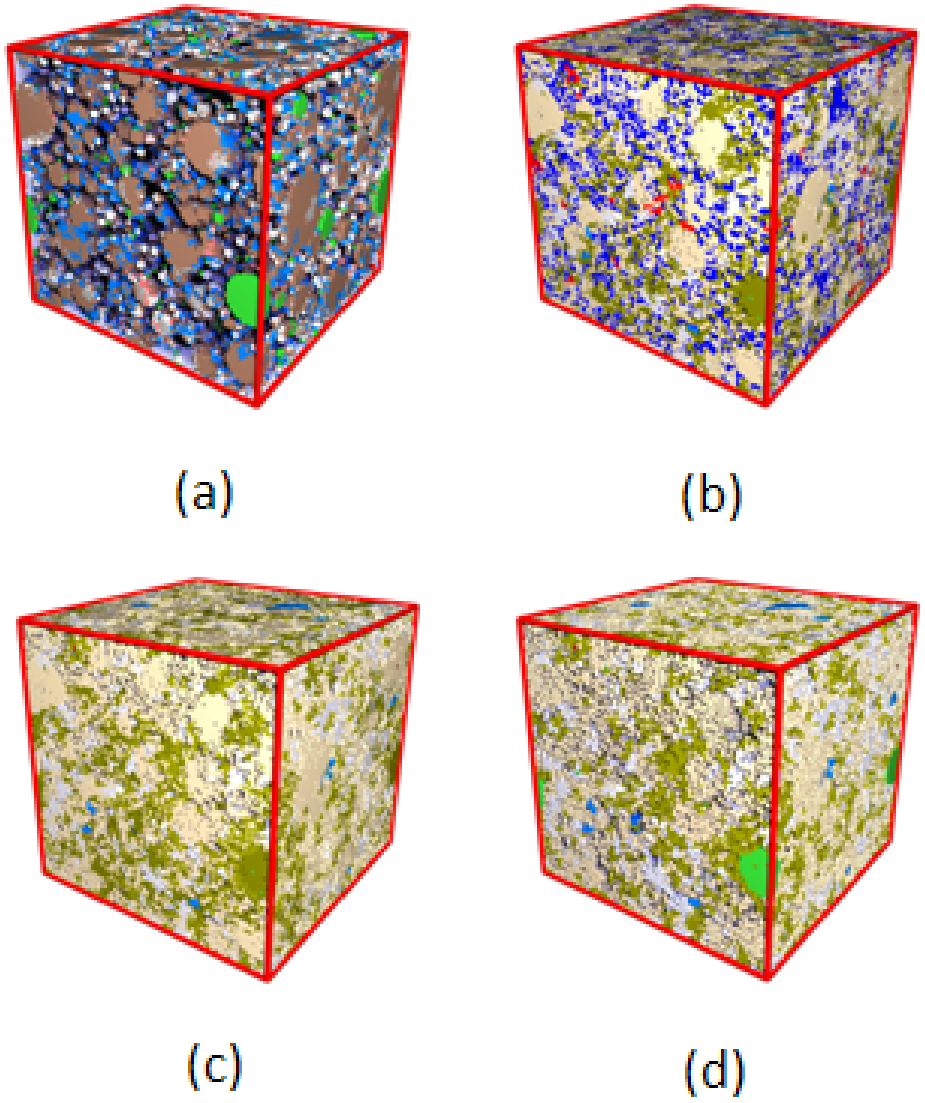

Figure 2: Microstructure development of hydration calculated by THAMES for a paste with w/c = 0.45: (a) initial microstructure; (b) hydration for 100 d (97 % degree of hydration); (c) leached until disappearance of portlandite; (d) continued leaching until equilibrium Ca concentration of 3 mmol/(kg water). Phase colors are C_3S = brown, C_2S = light blue, C_3A = dark grey, C_4AF = white, C–S–H = beige, CH = dark blue, calcite = green, ettringite and monosulfate = olive, hydrotalcite = light grey, capillary porosity = black.

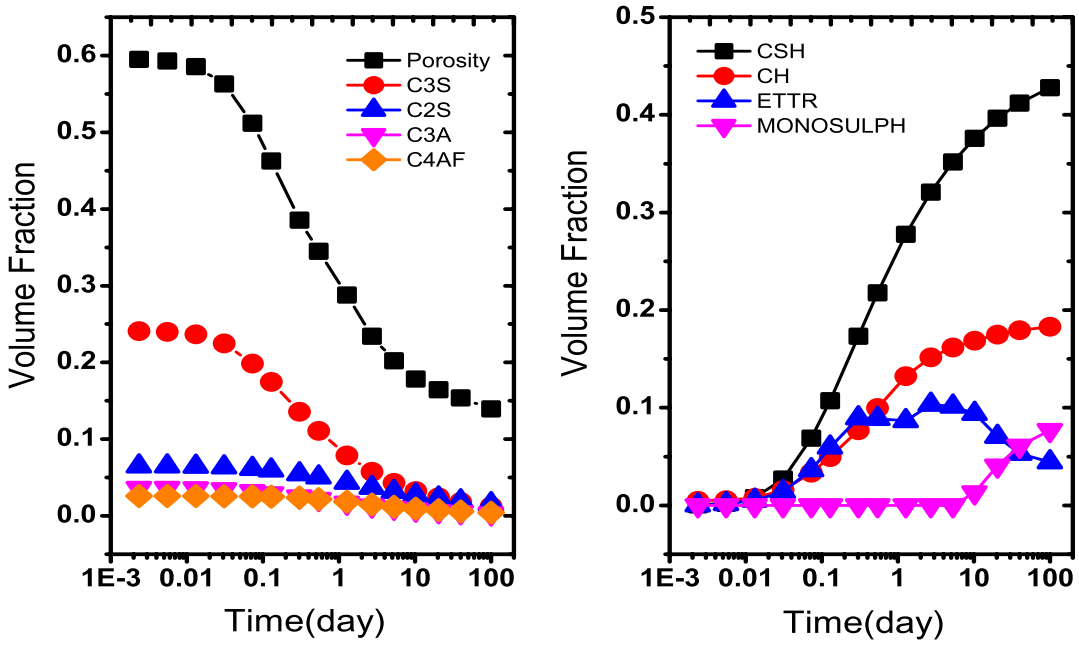

Figure 3: Solid phases in the cement paste (w/c = 0.45) during the 100 d hydration period, prior to leaching. (a) Capillary porosity and clinker phase volume fractions; and (b) major solid hydration products C–S–H, CH, ettringite, and monosulfate.

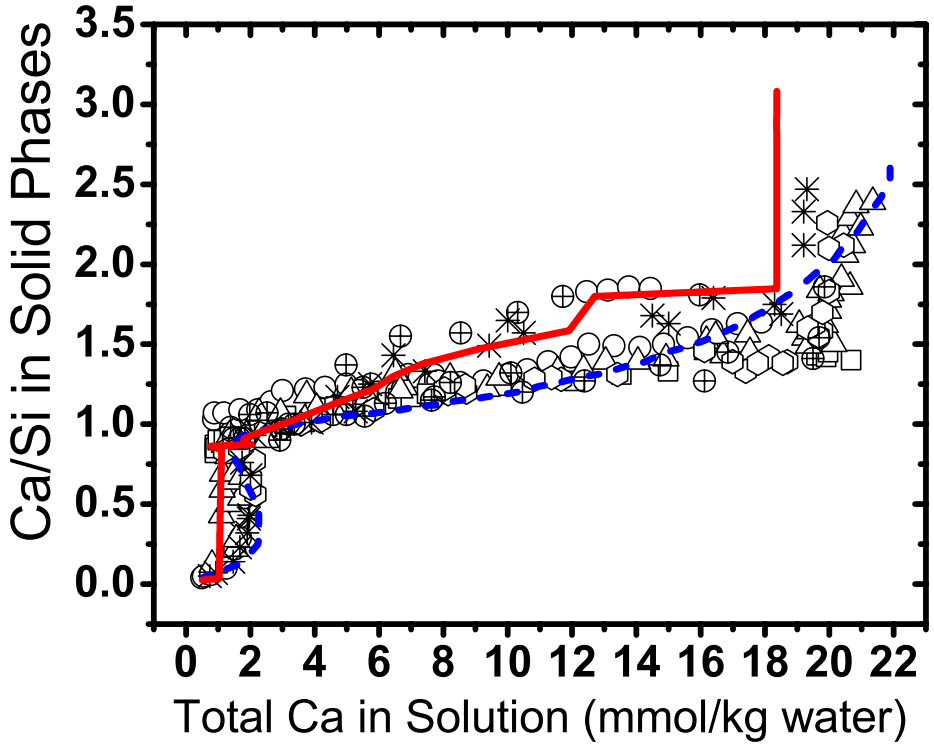

Figure 4: Calcium equilibrium between pore solution and solid phase, plotted as the equilibrium Ca/Si molar ratio of solids as a function of the total calcium concentration in solution. The solid curve is the current model's results; the dashed curve is predicted by Berner's model [13] for incongruent dissolution of C–S–H; points are measured by experiments on dissolution in pure calcium silicate systems as recorded in Ref. [14].

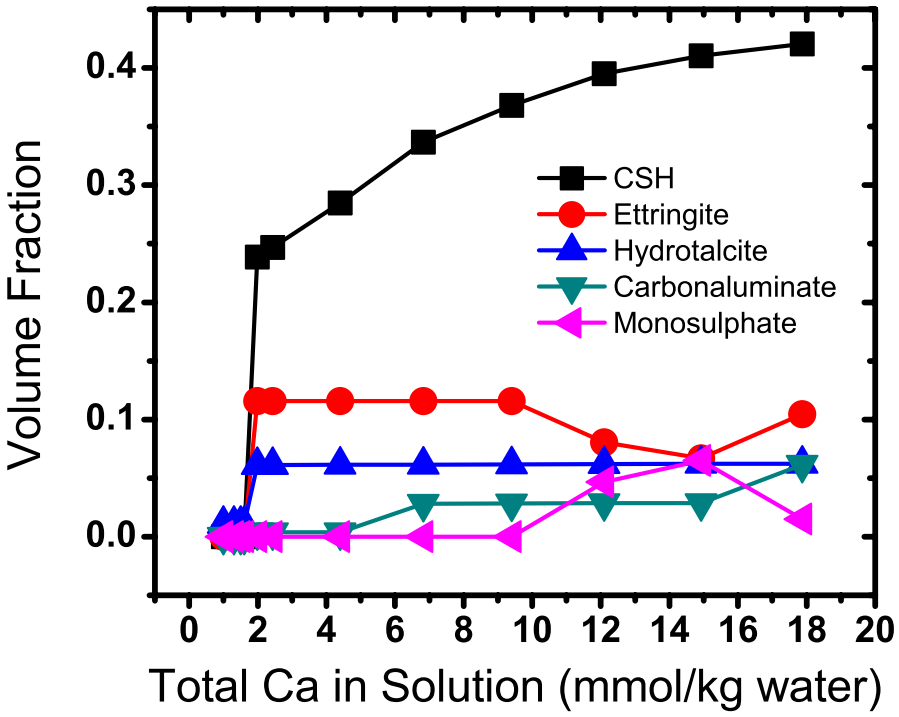

Figure 5: Equilibrium relationship between volume fraction of solid phases and total calcium in solution.

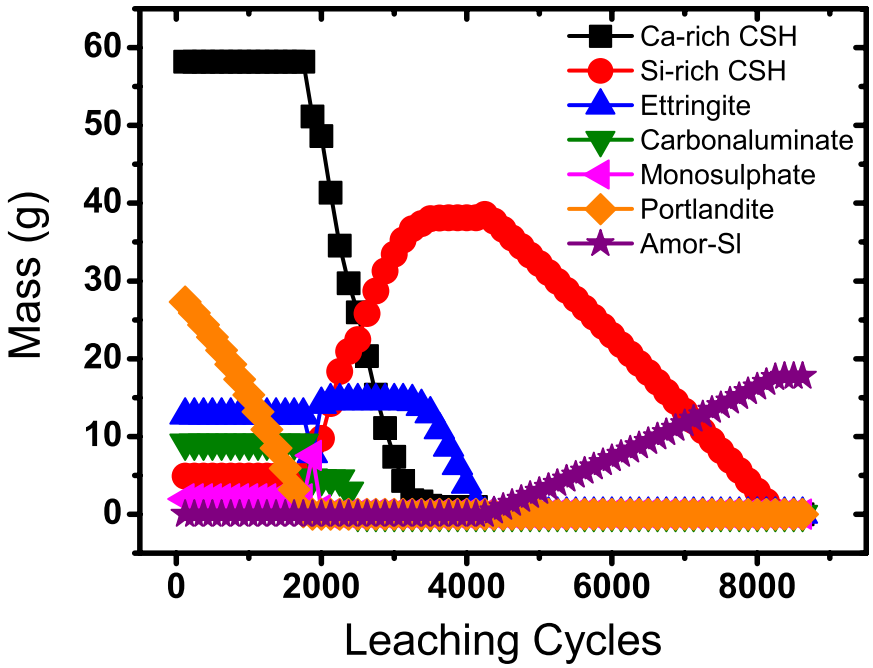

Figure 6: Predicted mass change of solid phases with increased leaching of a paste with w/c = 0.45.

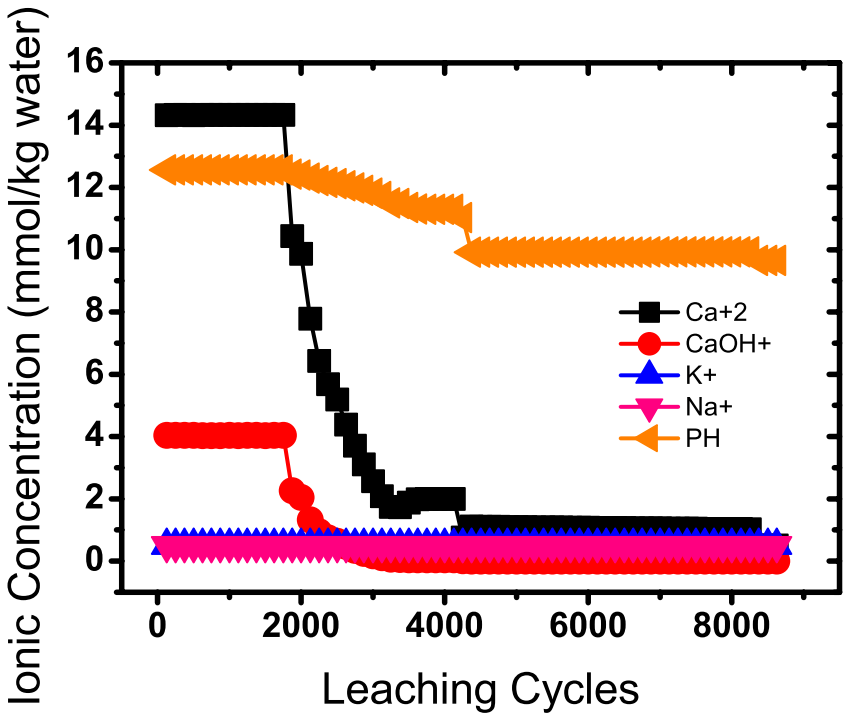

Figure 7: Predicted changes in provisional equilibrium solution concentrations at the end of each leaching cycle for a paste with w/c$\bar{0}$.45.

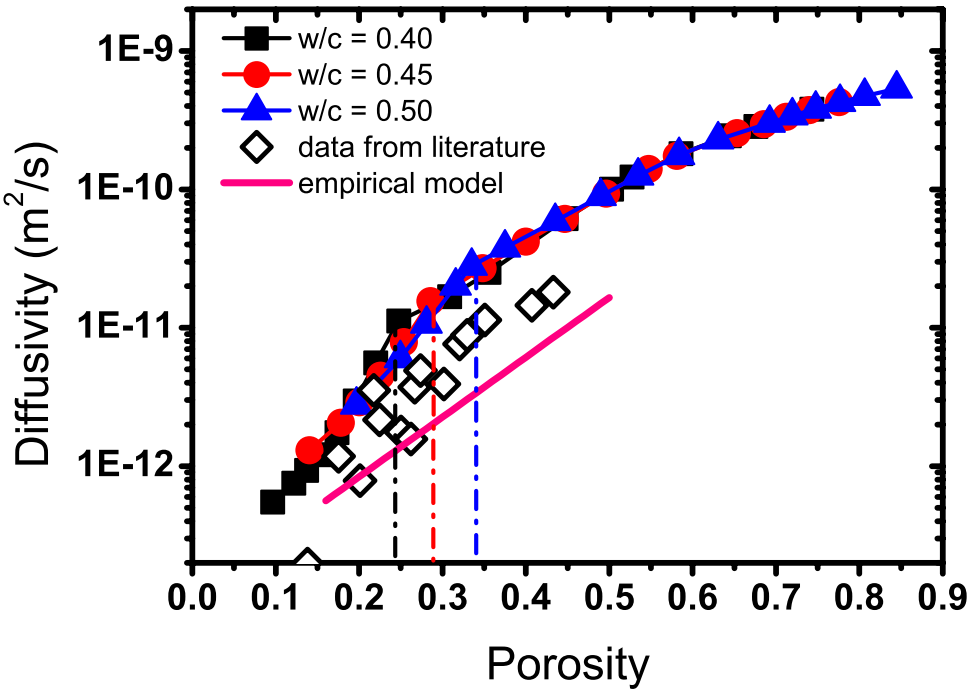

Figure 8: Effective diffusivity of the leached cement paste as a function of capillary porosity. Experimental measurements on a different portland cement paste with w/c = 0.4 and leached at 20 °C (open symbols) and an empirical model based on the same data (straight line), are taken from Ref. [15] and shown for comparison purposes only.

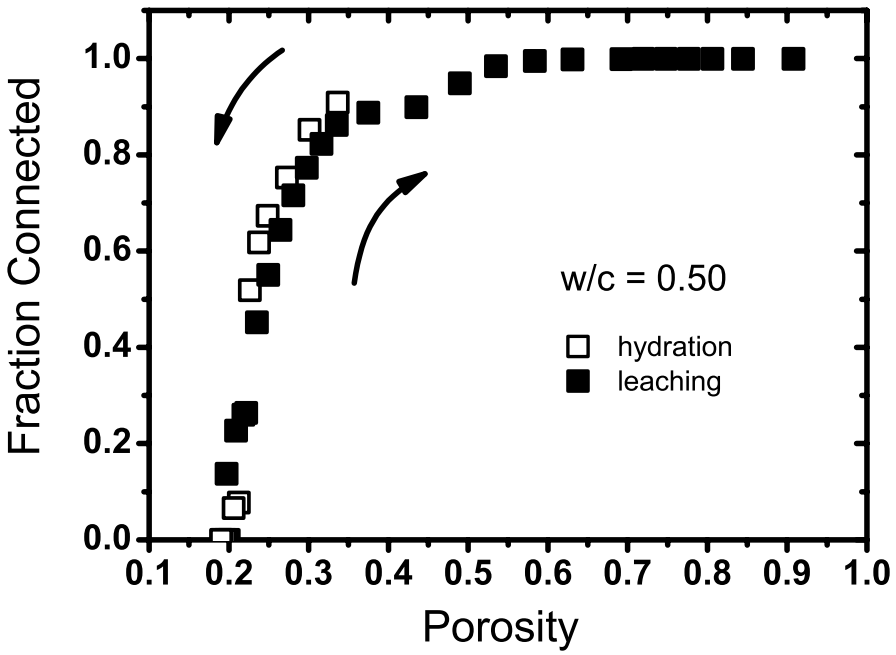

Figure 9: Fraction connected of capillary porosity versus capillary porosity for w/c = 0.50

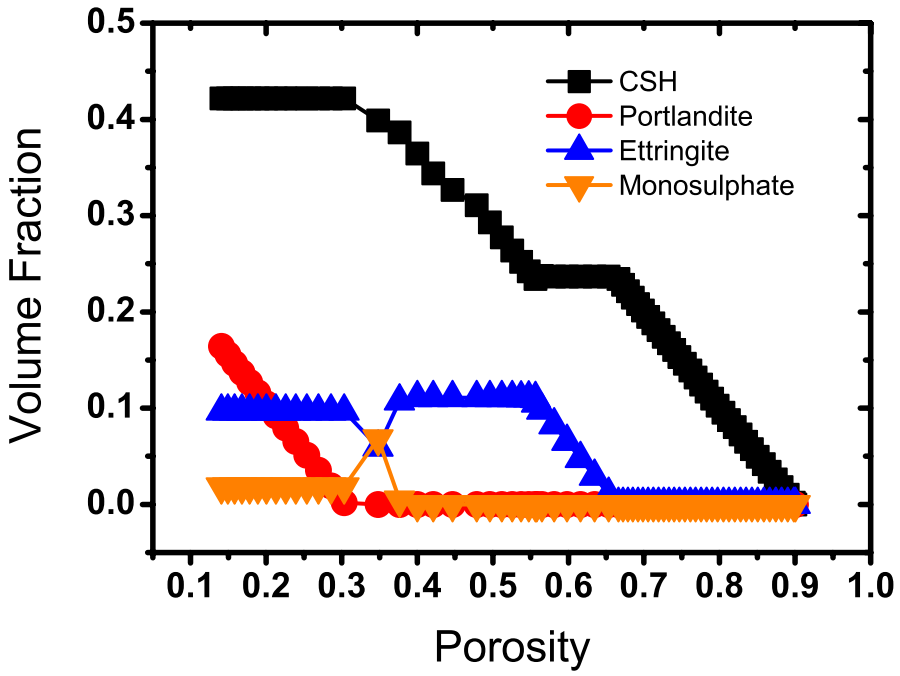

Figure 10: Volume fraction evolution of each phase as a function of porosity for w/c = 0.45.

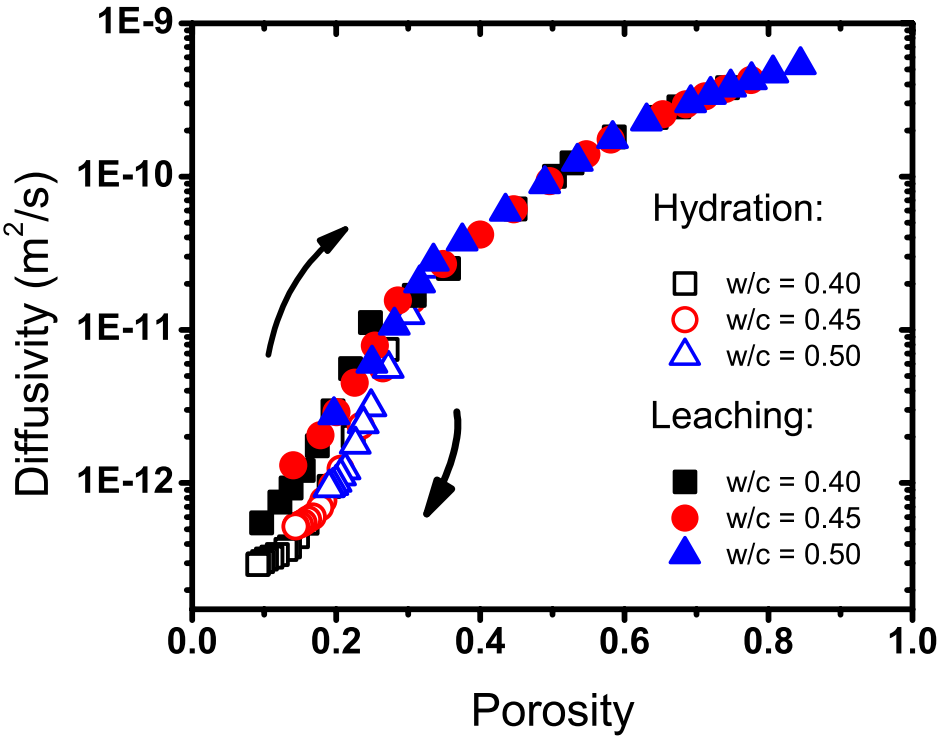

Figure 11: Effective diffusivity of cement pastes during hydration and leaching as a function of capillary porosity.

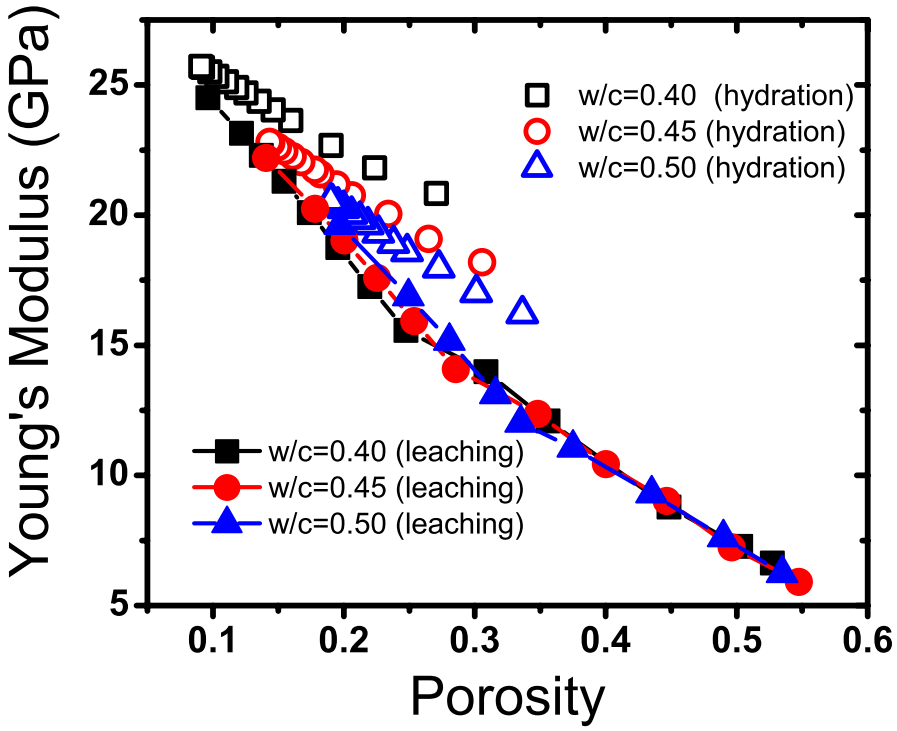

Figure 12: Calculated Young's modulus as function of porosity

List of Tables

Table 1: End member compositions, molar masses, and molar volumes used in the C–S–H solid solution model [30].

End Member	Composition	Molar Mass (kg/mol)	Molar Volume (10^{-5} m^3/mol)
Amorphous Silica	S	0.0609	2.9
Tobermorite-like C–S–H (Si-rich)	$C_{0.833}SH_{1.333}$	0.1308	5.87
Jennite-like C–S–H (Ca-rich)	$C_{1.667}SH_{3.833}$	0.2256	11.28

Table 2: Mineralogical composition of the simulated cement.

Phase/Mineral Name	**Mass Fraction (%)**
C_3S	54.5
β-C_2S	15.7
C_3A (cubic)	8.0
C_4AF	7.0
Bassanite (hemihydrate)	2.25
Anhydrite	0.19
Arcanite	1.07
Langbeinite	0.45
Aphthitalite	1.33
MgO (periclase)	3.2
$CaCO_3$ (calcite)	1.1
Present as solid solution in clinker phases	
Na_2O	0.11
MgO	0.7
SO_3	0.77

Table 3: Predicted volume fractions of porosity and solid hydration products at the end of the 100 d hydration period for cement pastes with w/c = 0.40, 0.45, and 0.50.

		Volume Fraction		
Phase/Mineral Name	**w/c =**	**0.40**	**0.45**	**0.50**
Capillary pores		0.089	0.139	0.186
C_3S		0.015	0.012	0.010
β-C_2S		0.017	0.016	0.015
C_3A (cubic)		0.003	0.003	0.003
C_4AF		0.005	0.004	0.004
C–S–H		0.456	0.428	0.403
CH		0.198	0.183	0.170
Ettringite		0.024	0.044	0.058
Monosulfate		0.093	0.077	0.065
Calcite		0.031	0.029	0.027
Hydrotalcite		0.068	0.064	0.059
Degree of Hydration		0.897	0.901	0.905